Resonant photoemission of oxidized Yb: Experiment and theory

J. Schmidt-May and F. Gerken
II. Institut für Experimentalphysik, Universität Hamburg, D-2000 Hamburg 50, Germany

R. Nyholm
Institute of Physics, University of Uppsala, P.O. Box 530, S-751 21 Uppsala, Sweden

L. C. Davis
Research Staff, Ford Motor Company, Dearborn, Michigan 48121-2053
(Received 8 May 1984)

The oxidation-induced valence change of Yb leads to a single $4f$ hole in the ground state. The creation of the $4f^{13}$ configuration which does not exist for any pure rare-earth metal makes it possible to analyze the $4d \rightarrow 4f$ Fano resonance for a simple system experimentally as well as theoretically. Calculated Fano profiles for the $4f^{12}$ final-state multiplets are in good agreement with photoemission measurements taken with the FLIPPER monochromator at Hamburger Synchrotronstrahlungslabor, Deutsches Elektronen-Synchrotron, using synchrotron radiation from the storage ring DORIS.

I. INTRODUCTION

The interaction of oxygen with Yb is of special interest since the oxidation induces a valence change of the divalent Yb with a closed $4f$ shell. Thus the oxidation opens the $4f$ shell leading to a $4f^{13}$ ground-state configuration which does not exist for any pure rare-earth (RE) metal. Moreover, it is possible to follow the Fano-type[1] resonance in the vicinity of the $4d \rightarrow 4f$ excitation in the oxide. This resonance has already been observed in photoelectron spectroscopy[2] as well as in energy-loss experiments.[3] In this paper we will give a detailed experimental and theoretical analysis of this resonance phenomenon.

The techniques of constant initial-state (CIS) and constant final-state (CFS) spectroscopy have successfully been applied to the series of the RE elements to follow the $4d \rightarrow 4f$ resonance.[4] Gerken *et al.*[5] have, for some cases, determined the partial cross section of different subshells contributing to the resonance. Here we will concentrate on the $4f$ shell. Since the resonance behavior of the $4f$ states strongly depends on the initial occupation number of the $4f$ shell, resonant photoemission can even be used to identify reaction products according to the valencies of the RE atoms[6] involved. In the case of oxidized Yb we have a comparably simple system, Yb_2O_3. The resonance originates from the interference of the direct emission of a $4f$ electron from the $4d^{10}4f^{13}$ ground state with the decay of the excited discrete $4d^{9}4f^{14}$ state. In this paper experimental CIS spectra with different initial energies in the $4f$ region will be presented and compared to model calculations for all $4f^{12}$ final-state multiplets (see Sec. IV). The calculations will be described in Sec. III.

II. EXPERIMENT AND RESULTS

The experiments were carried out at the Hamburger Synchrotronstrahlungslabor, Deutsches Elektronen-Synchrotron, with the FLIPPER monochromator.[7] Details concerning the photoemission setup and procedures for the determination of the transmission of the double-pass cylindrical mirror analyzer to correct the energy-distribution curves (EDC's) and, here, more important, the CIS spectra are given elsewhere.[8] The overall resolution of the monochromator and the analyzer in the spectra shown here was 0.2—0.5 eV. The sample was prepared by evaporation of high-purity Yb (99.99%) from tungsten baskets onto a stainless-steel substrate. The base pressure during measurements was lower than 2×10^{-10} Torr. During evaporation the pressure rose to $(2-4)\times10^{-9}$ Torr. The clean metal surface was oxidized by exposure to high-purity oxygen (99.998%) for 100 sec at 1×10^{-6} Torr.

The multiplet structure and photoemission intensities of the $4f^{N} \rightarrow 4f^{N-1}$ transition have been calculated in inter-

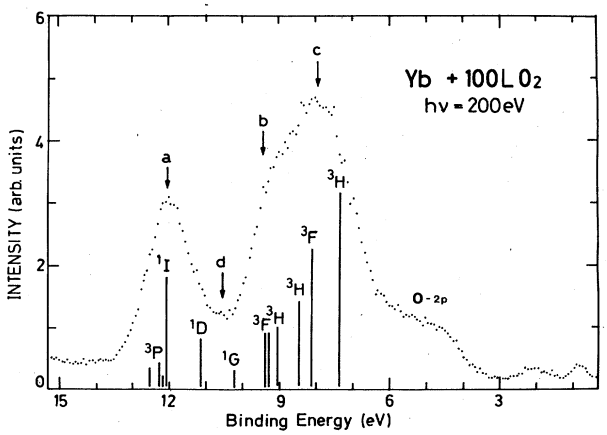

FIG. 1. EDC of oxidized Yb recorded with 200-eV photon energy. [1 langmuir (L)$\equiv 10^{-6}$ Torr sec.]

mediate coupling for all RE's by Gerken.[9] Figure 1 shows the result for the $4f^{13} \rightarrow 4f^{12}$ transition together with an EDC recorded at 200-eV photon energy, i.e., about 20 eV above resonance energy. The $4f$ emission is dominated by two structures at around 8- and 12-eV binding energy, the latter mainly caused by the ^1I multiplet. The shoulder at ~ 5 eV is due to the emission from the oxygen $2p$ band. At low photon energies (typically 40 eV, not shown here) it is the prominent structure and smears out the whole $4f$ emission. Since the width of the O-$2p$ band is several eV and its photoemission intensity is not negligible even at 200 eV, the $4f$ structure is still influenced. The $4f^{12}$ multiplets are better resolved in case that no band emission is present as, for example, in intermetallic mixed-valence Yb/Al compounds.[10] We found the same resonance behavior of the $4f^{12}$ structure in Yb/Al, and the comparison with the model described below could be done analogously.

At resonance the multiplet structure with the highest binding energy shows the strongest resonance (see Fig. 2). As it will turn out from the calculations it is the ^1I state which is almost exclusively responsible for this resonance since the ^3P does not contribute. Another way to obtain information about the resonance, other than by recording EDC's at various photon energies, is to follow the resonance by CIS spectra, i.e., recording the intensity variation at a constant binding energy (initial energy) while continuously tuning the photon energy. In Fig. 3 we show several CIS spectra for different initial energies as indicated by labels a–d in Fig. 1. These CIS spectra are fully corrected for the incoming photon flux and analyzer transmission and are directly comparable in intensity. They reflect the resonance behavior of different $4f^{12}$ final states. As already obvious from the EDC's in Fig. 2 the ^1I shows the strongest resonance (curve a in Fig. 3). For comparison, a CFS spectrum with a final energy of 5 eV is included in Fig. 3 (not in the same intensity scale).

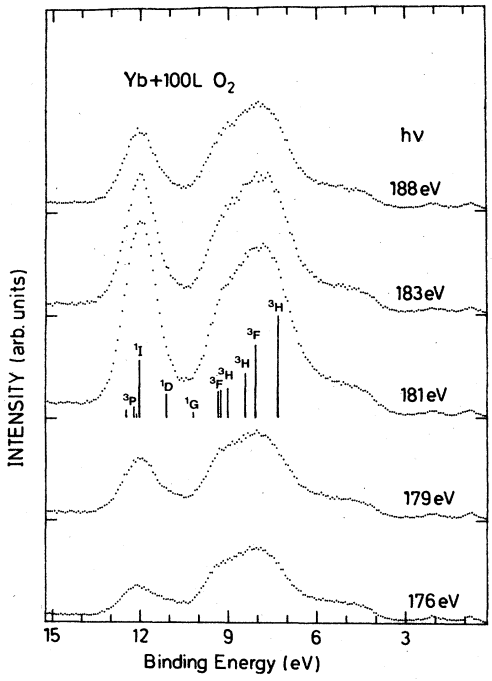

FIG. 2. EDC's for different photon energies at resonance comparable in intensity.

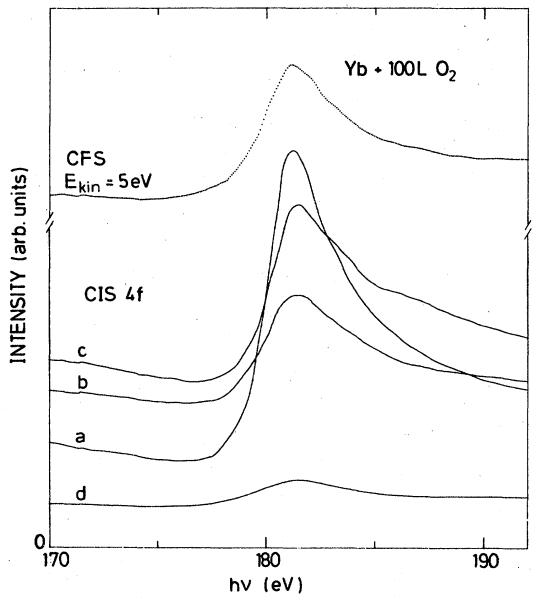

FIG. 3. CIS spectra for different initial energies within the $4f$ region (a-d, see Fig. 1) and a yield spectrum with an electron energy of 5 eV.

III. THEORY

In this section we present a theoretical model to which the data on oxidized Yb can be compared. The model assumes that we can treat the relevant electron states (e.g., $4f$ and $4d$) as atomic, even though the experiment was done for a solid. The orbitals are well localized, so we expect this to be a good approximation. Off resonance, the photoemission is mainly due to $4f \rightarrow \epsilon l$ transitions, where ϵl is a continuum orbital. The final ionic states are the multiplets of the f^{12} configuration. This is a nice example to study because the atomic configurations are simple and the photoabsorption fits a Fano[1] line shape.

The resonance in the photoemission intensity occurs when the photon energy $h\nu$ equals the $4d \rightarrow 4f$ transition energy $E_0 = 180.5$ eV. One of the fundamental assumptions made here is that most of the $4d \rightarrow f$ oscillator strength is in this transition. This appears to be the case for all but the lightest rare earths. In Ce, for example, much of the oscillator strength lies above the continuum threshold. The resonance is broad and involves a collective oscillation of the outer electrons. It is necessary to use a self-consistent-field approximation [e.g., time-dependent local-density approximation of Zangwill and Soven[11]] or more general many-body techniques (Wendin,[12] Dehmer *et al.*,[13] Starace[14]). For the problem considered in this paper, no such treatment is required; a Hartree-Fock calculation with the appropriate treatment of angular momentum coupling appears to be sufficient.

The resonance is similar in many respects to the behavior of the heavy $3d$ metals.[15–18]

The analysis of the resonance involves the interaction of discrete states having configuration d^9f^{14} with the continuum final states $d^{10}f^{12}\epsilon l$. We use the formalism of Davis and Feldkamp[19,20] which is a generalization of the original work of Fano.[1] The ground state Φ_g is $f^{13}(j_0,m_{j_0})$ where $j_0=\frac{7}{2}$. Dipole selection rules limit the discrete states ϕ_n to $j=\frac{5}{2}$ only. We include the effects of spin-orbit (SO) interaction in Φ_g and ϕ_n since it is necessary and straightforward to do so. In the final states, however, it becomes more difficult to treat SO in the present context, so we neglect it in the $4f$ shell. The only effect of this approximation is that the emission is distributed among several final states somewhat differently than predicted. As a consequence, we must compare to experiment only certain total intensities that are unaffected (e.g., $^3H+^3F+^1G$).

The final states are found by coupling the orbital angular momentum L_f of the f^{12} ion to the l of the photoelectron, giving a total L for the system. Likewise, the spin S_f of the ion is coupled to that of the photoelectron to give total spin S. The total angular momentum J is the vector sum of L and S. Now ϕ_n interacts only with continua with $J=\frac{5}{2}$, $L=2$, and $S=\frac{1}{2}$ because the interaction conserves angular momentum and spin. The matrix element V_{kn} is the same as in super-Coster-Kronig (sCK) transitions,[21] typically $R_K(4d,\epsilon l;4f,4f)$ (see the Appendix). The other final states contribute to the emission, but do not show any resonance behavior.

The intensity of any final state ψ_k is proportional to the absolute square of the amplitude

$$D=A+B(q-i)/(\epsilon+i)\ , \tag{1}$$

where

$$A=\langle\psi_k\mid T\mid\Phi_g\rangle\ , \tag{2}$$

$$B=\sum_{k',n}(\pi V_{kn}V_{k'n}/\Gamma)\langle\psi_{k'}\mid T\mid\Phi_g\rangle\ , \tag{3}$$

and

$$\epsilon=(h\nu-E_0)/\Gamma\ . \tag{4}$$

The Fano profile index q involves V_{kn} and dipole matrix elements $(\epsilon l\mid r\mid 4f)$ and $(4f\mid r\mid 4d)$ (see the Appendix).

The absorption of photons, which is equal to the sum over all final states of the photoemission intensity, has the familiar form

$$\mu=\mu_0+\mu_1(q+\epsilon)^2/(\epsilon^2+1)\ . \tag{5}$$

Similarly, from Eq. (1), we find that the intensity N_k can be written in the same form but with an effective q which depends upon the particular final state,

$$N_k=N_{k0}+N_{k1}(q_k+\epsilon)^2/(\epsilon^2+1)\ , \tag{6}$$

where

$$q_k=-p+(p^2+1)^{1/2} \tag{7}$$

and

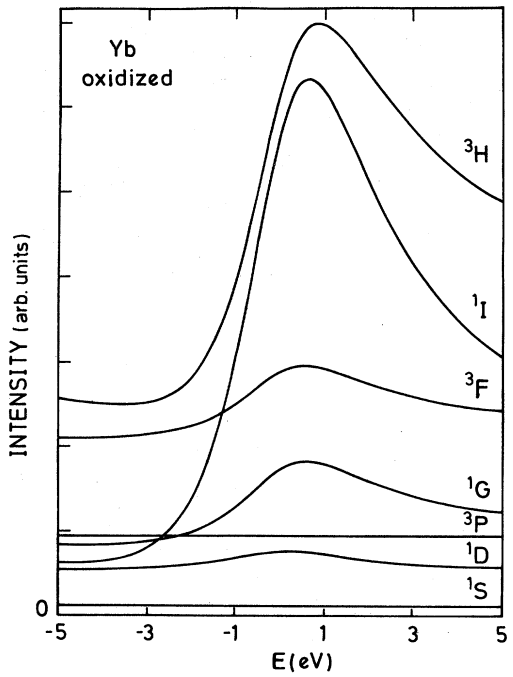

FIG. 4. Calculated intensity profiles of all multiplets of the $4f^{12}$ final state.

$$p=[A^2-q^2B^2-(A-B)^2]/(2ABq)\ . \tag{8}$$

Note that the full width at half maximum width $2\Gamma=2\pi\sum_k V_{kn}^2$ is the same for all final states and is independent of $n=m_j$.

To evaluate the various matrix elements appearing in the equations above, we started with numerical wave functions from a Herman-Skillman[22] code. (Calculations were done for Tm which has a ground-state configuration $4f^{13}6s^2$.) The resulting q and Γ were within a factor of 2 of the results determined by Johansson *et al.*[2] We then scaled the radial matrix elements, one factor for the sCK matrix elements and another for the ratio of dipole matrix elements, to give q and Γ values in agreement with our experimental results for the ^1I. Having thus determined all matrix elements, we then calculated the total intensity for each final-state multiplet $f^{12}(L_f,S_f)$. The intensity involved a sum over l, L, S, J, and M_J and an average over m_{j_0} and polarization of the photon. The results are displayed in Fig. 4 and in Table I.

TABLE I. Calculated effective q values for Yb $4f^{12}$ final states.

State	q
^1I	2.60
^3H	1.96
^1G	2.86
^3F	3.10
^1D	9.2
$^3H+^3F+^1G$	2.19
Total	2.41

IV. DISCUSSION

The ^1I intensity goes through the largest resonance. Fortunately, these states are not strongly mixed with any other (L_f,S_f) final states, so scaling the matrix elements to give agreement with the measured ^1I intensity is meaningful. The experimental result in Fig. 5 fits a Fano line shape with $q=2.6$ and $\Gamma=1.8$ eV. On the other hand, the states ^3H, ^3F, and ^1G are strongly mixed by SO. The amount of mixing is demonstrated by comparing the intensities in LS coupling (see Ref. 23, Table 4, p. 79) to those in intermediate coupling (see Table 2d in Ref. 9). For example, the ^1G intensity is reduced by a factor of almost 6 in the latter, with its intensity being distributed to ^3H and ^3F. As indicated in Fig. 1, these states also overlap in energy. Since the total is invariant, we added the separate intensities and found that the theoretical effective $q=2.19$ fitted the data well [see Fig. 6(a)]. In addition we found that the theoretical change in intensity (maximum minus minimum) at resonance is 1.1 times that of ^1I, which compares reasonably well with the experimental value of 1.2 deduced from corresponding EDC's.[24] The ^1D intensity is weakly resonant, which is also consistent with experiment (see Fig. 3). The lack of resonance in the ^3P and ^1S intensities can be understood as follows. Only ϵg has large sCK matrix elements and the decay of $4d^94f^{14}(^2D)$ into $4d^{10}4f^{12}(^3P$ and $^1S)$ ϵg is forbidden by conservation of angular momentum.

The calculated $4f$ yield, i.e., the sum of all individual terms of the $4f^{12}$ final state, with an effective $q=2.41$, is also in quite good agreement with the sum of all CIS curves [Fig. 6(b)]. The calculated yield cannot fit the experimental CFS curve since the latter contains more than the decay of the discrete $4d^94f^{14}$ state by the emission of a $4f$ electron leading to the $4d^{10}4f^{12}$ final states. The energy in the direct-recombination process may be transferred to electrons of other shells:

$$4d^95s^25p^64f^{14}\rightarrow\begin{cases}4d^{10}5s\,5p^64f^{13}+\epsilon l\\ 4d^{10}5s^25p^54f^{13}+\epsilon l\\ 4d^95s^25p^64f^{13}+\epsilon l\ ,\end{cases}$$

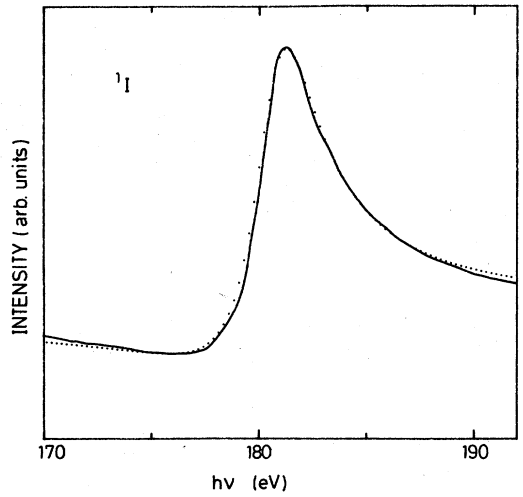

FIG. 5. Experimental CIS curve (——) and Fano fit (· · · ·) with $q=2.6$ and $\Gamma=1.8$ eV.

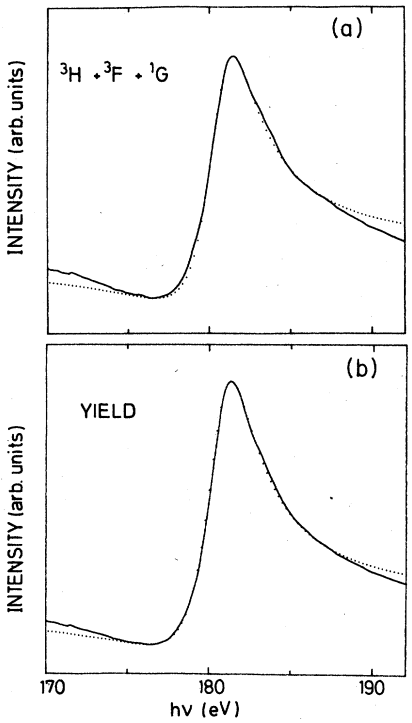

FIG. 6. (a) Sum of CIS spectra b and c (——) compared with the calculated Fano profile of $^3H+^3F+^1G$ (· · · ·, $q=2.19$). (b) Sum of all CIS spectra (——) compared with calculated $4f$ yield (· · · ·, $q=2.41$). The calculated curves used theoretical q values, but the vertical scale was adjusted to fit the experimental data.

where the last decay corresponds to the direct photoemission of a $4d$ electron. Additionally the valence electrons taking part in the oxygen bonding may contribute to the decay. Indeed, we observed experimentally an enhancement of the $5s$ and $5p$ emission when tuning the photon energy through the resonance (not shown here). Unfortunately we cannot decompose the partial yield as Gerken *et al.*[5] did for several RE metals since the Auger structures are broad and the direct $4d$ emission cannot be accurately determined close to threshold.

V. CONCLUSION

The present work demonstrates the resonance behavior of the $4f$ emission in the $4d\rightarrow4f$ excitation region of oxidized Yb to be in close correspondence with Hartree-Fock model calculations. The progress in high-resolution photoemission provides information about the contribution of different $4f$ multiplets of the same final state to the Fano resonances in RE metals and their compounds. Further developments have to be done to determine all contributing decay channels with sufficient accuracy especially in case of more complicated systems.

ACKNOWLEDGMENTS

This work was supported by the Bundesministerium für Forschung und Technologie from funds for research with synchrotron radiation and the Swedish Natural Science Research Council.

APPENDIX

In this appendix, detailed expressions for the matrix elements appearing in Sec. III are given. Let Φ denote a state with filled $4d$ and $4f$ shells. The ground state ($4d^{10}4f^{13}$ configuration) is

$$\Phi_g = f_{j_0 m_{j_0}} | \Phi \rangle, \quad j_0 = \tfrac{7}{2} . \tag{A1}$$

We use the notation where, for example, $f_{j_0 m_{j_0}}$ means an annihilation operator for a $4f$ state with quantum numbers j_0 and m_{j_0}.

The discrete states ($4d^9 4f^{14}$ configuration) are

$$\phi_n = d_{jm_j} | \Phi \rangle , \tag{A2}$$

where just $j = \frac{5}{2}$ is used since only $\frac{7}{2} \to \frac{5}{2}$ is allowed. The continuum states ($4d^{10}4f^{12}(L_f,S_f)\epsilon l$) are

$$\begin{aligned}\psi_{kE} = \sum_{M_L, M_S} \langle L\, S\, M_L\, M_S | J\, M_J \rangle \sum_{\substack{m_l, m_s, \\ M_{Lf}, M_{Sf}}} & \langle l\, L_f\, m_l\, M_{Lf} | L\, M_L \rangle \langle \tfrac{1}{2}\, S_f\, m_s\, M_{Sf} | S\, M_S \rangle \\ & \times l^{\dagger}_{m_l m_s} \sum_{\substack{m_1, \sigma_1 \\ m_2, \sigma_2}} \langle 3\,3\, -m_1\, -m_2 | L_f\, M_{Lf} \rangle \langle \tfrac{1}{2}\, \tfrac{1}{2}\, -\sigma_1\, -\sigma_2 | S_f\, M_{Sf} \rangle \\ & \times (2)^{-1/2} (-1)^{m_1 + m_2 + \sigma_1 + \sigma_2} f_{m_1 \sigma_1} f_{m_2 \sigma_2} | \Phi \rangle ,\end{aligned} \tag{A3}$$

where $l^{\dagger}_{m_l m_s}$ is a creation operator for a continuum orbital ϵl with $l_z = m_l$ and $s_z = m_s$ and where $f_{m\sigma}$ annihilates a $4f$ orbital with $l_z = m$ and $s_z = \sigma$.

The super-Coster-Kronig matrix element is

$$\begin{aligned}V_{kn} = \langle \psi_{kE} | H | \phi_n \rangle = & 7(2l+1)^{1/2}(2S_f+1)^{1/2}(2L_f+1)^{1/2}(-1)^{-j-m_j+L_f} \\ & \times \sum_K \frac{e^2}{2K+1} R_K(4d, \epsilon l; 4f, 4f)(-1)^K \langle 2\,3\,0\,0 | K\,0 \rangle \langle l\,3\,0\,0 | K\,0 \rangle \begin{Bmatrix} 3 & K & 2 \\ l & L_f & 3 \end{Bmatrix} .\end{aligned} \tag{A4}$$

Here $\{^{j_1\, j_2\, j_3}_{J_1\, J_2\, J_3}\}$ is a $6j$ symbol and (A4) holds for $L = 2$, $S = \frac{1}{2}$, $J = j$, and $M_j = -m_j$. Otherwise, $V_{kn}(E)$ vanishes.

The dipole transition matrix element for $S = \frac{1}{2}$ and $x = 0, \pm 1$ is

$$\begin{aligned}\langle \psi_{kE} | T^{(1)}_x | \Phi_g \rangle = & (2j_0+1)^{1/2}(2S_f+1)^{1/2}(2L+1)^{1/2}(2L_f+1)^{1/2} \langle \epsilon l || T^{(1)} || 4f \rangle \\ & \times \begin{Bmatrix} 3 & 1 & L \\ l & L_f & 3 \end{Bmatrix} \begin{Bmatrix} J & 1 & j_0 \\ 3 & \frac{1}{2} & L \end{Bmatrix} \langle j_0\, 1\, -m_{j_0}\, x | J M_J \rangle (-1)^{m_{j_0} + 1/2 - S_f + l + L + 2J} ,\end{aligned} \tag{A5}$$

where

$$\begin{aligned}\langle \epsilon l || T^{(1)} || 4f \rangle &= 7^{1/2} \langle 3\,1\,0\,0 | l\,0 \rangle (\epsilon l | r | 4f) \\ &= -(3)^{1/2} (\epsilon d | r | 4f), \quad l = 2 \\ &= 2(\epsilon g | r | 4f), \quad l = 4 .\end{aligned} \tag{A6}$$

The dipole matrix element (A5) is nonzero for $S = \frac{1}{2}$ and $l = 2$ or 4. Also,

$$\langle \phi_n | T^{(1)}_x | \Phi_g \rangle = -\langle 4f || T^{(1)} || 4d \rangle (2j_0+1)^{1/2} \begin{Bmatrix} j & 1 & j_0 \\ 3 & \frac{1}{2} & 2 \end{Bmatrix} \langle j_0\, 1\, -m_{j_0}\, x | j\, -m_j \rangle (-1)^{x + 1/2 - j} , \tag{A7}$$

where

$$\langle 4f || T^{(1)} || 4d \rangle = 3^{1/2} (4f | r | 4d) . \tag{A8}$$

Neglecting the difference between $\bar{\phi}_n$ and ϕ_n, we find the profile index q_n (not to be confused with q_k in Sec. III) to be[19]

$$q_n = \langle \phi_n | T^{(1)}_x | \Phi_g \rangle \Big/ \left[\pi \sum_k V_{kn}(E) \langle \psi_{kE} | T^{(1)}_x | \Phi_g \rangle \right] . \tag{A9}$$

This reduces for $j=\frac{5}{2}$ to

$$q_n = q = -\langle 4f||T^{(1)}||4d\rangle \Big/ \left[\pi \sum_{l,L_f,S_f} 7(2l+1)^{1/2}(2S_f+1)^{1/2}(2L_f+1)^{1/2}\langle \epsilon l||T^{(1)}||4f\rangle \right.$$
$$\times \begin{Bmatrix} 3 & 1 & 2 \\ l & L_f & 3 \end{Bmatrix} (-1)^{S_f+l+L_f} \sum_K \frac{e^2}{2K+1} R_K(4d,\epsilon l;4f,4f)$$
$$\left. \times (-1)^K \langle 2\,3\,0\,0\,|\,K\,0\rangle \langle l\,3\,0\,0\,|\,K\,0\rangle \begin{Bmatrix} 3 & K & 2 \\ l & L_f & 3 \end{Bmatrix} \right], \tag{A10}$$

which is independent of m_{j_0}, m_j, and x.

[1]U. Fano, Phys. Rev. **124**, 1866 (1961).

[2]L. I. Johansson, J. W. Allen, I. Lindau, M. H. Hecht, and S. B. M. Hagström, Phys. Rev. B **21**, 1408 (1980). For a detailed UPS study of the initial oxidation of Yb metal with a photon energy far below the resonance, see Y. Takakuwa, S. Suzuki, T. Yokokutsa, and T. Sagawa, J. Phys. Soc. Jpn. **53**, 687 (1984).

[3]E. Bertel, G. Strasser, F. P. Netzer, and J. A. D. Matthew, Surf. Sci. **118**, 387 (1982).

[4]F. Gerken, Ph.D. thesis, University of Hamburg, 1982.

[5]F. Gerken, J. Barth, and C. Kunz, *X-Ray and Atomic Inner-Shell Physics—1982 (International Conference, University of Oregon),* proceedings of the International Conference on X-Ray and Atomic Inner-Shell Physics, edited by Bernd Crasemann (AIP, New York, 1982), p. 602.

[6]J. Barth, F. Gerken, J. Schmidt-May, A. Flodström, and L. I. Johansson, Chem. Phys. Lett. **96**, 532 (1983).

[7]J. Barth, F. Gerken, C. Kunz, and J. Schmidt-May, Nucl. Instrum. Methods **208**, 307 (1983).

[8]J. Barth, F. Gerken, and C. Kunz, Nucl. Instrum. Methods **208**, 797 (1983).

[9]F. Gerken, J. Phys. F **13**, 703 (1983).

[10]R. Nyholm, I. Chorkendorff, and J. Schmidt-May, Surf. Sci. **143**, 177 (1984).

[11]A. Zangwill and P. Soven, Phys. Rev. Lett. **45**, 204 (1980).

[12]G. Wendin, Struct. Bonding (Berlin) **45**, 1 (1981).

[13]J. L. Dehmer, A. F. Starace, U. Fano, J. Sugar, and J. W. Cooper, Phys. Rev. Lett. **26**, 1521 (1971).

[14]A. F. Starace, Appl. Opt. **19**, 4051 (1980).

[15]R. Bruhn, B. Sonntag, and H. W. Wolff, J. Phys. B **12**, 203 (1979).

[16]R. Bruhn, E. Schmidt, H. Schröder, and B. Sonntag, Phys. Lett. **90A**, 41 (1982).

[17]E. Schmidt, H. Schröder, B. Sonntag, H. Voss, and H. E. Wetzel, J. Phys. B **16**, 2961 (1983).

[18]L. C. Davis and L. A. Feldkamp, Phys. Rev. A **17**, 2012 (1978).

[19]L. C. Davis and L. A. Feldkamp, Phys. Rev. B **15**, 2961 (1977).

[20]L. C. Davis and L. A. Feldkamp, Phys. Rev. B **23**, 6239 (1981).

[21]E. J. McGuire, Phys. Rev. A **5**, 1043 (1972).

[22]F. Herman and S. Skillmann, *Atomic Structure Calculations* (Prentice-Hall, Englewood Cliffs, New Jersey, 1963).

[23]P. A. Cox, Struct. Bonding (Berlin) **24**, 59 (1975).

[24]In the present case we find that the relative intensities between the sum of CIS curves *b* and *c* and CIS curve *a* give the same result which also justifies one to use the sum of all CIS curves as a measure for the total $4f$ yield.